The Use of Piezoceramic Transducers for Smart Structural Testing

Bor-Tsuen Wang* and Rong-Liang Chen

Department of Mechanical Engineering
National Pingtung University of Science and Technology
Pingtung, Taiwan 91207, R.O.C.

ABSTRACT

This paper presents the use of piezoceramic transducers, PZT actuators and PVDF sensors, for experimental modal testing of a simply supported plate. A series of rectangular shape of PVDF films are evenly distributed over the plate and act as the sensing devices instead of traditional acceleration sensors. The rectangular PZT patches that are adhered to the opposite surfaces of the plate and activated 180° out-of-phase for pure bending excitation are adopted as the actuator. The theoretical formulation of frequency response functions (FRFs) of the piezoceramic transducers is developed. The mode shape functions of the PZT actuator and the PVDF sensor are identified, respectively. Experiments are performed to obtain a column of FRF matrix. The structural modal parameters, including natural frequencies, modal damping ratios and mode shapes, can then be extracted by a modal parameter extraction method. Results show the modal parameters can be properly obtained and physically interpreted in comply with theoretical results. This paper presents the concepts of smart structural testing (SST) with the use of piezoceramic transducers and leads to the applications of smart structures to health monitoring of structural systems.

Keywords: piezoceramic transducer, PZT actuator, PVDF sensor, modal testing, simply supported plate, natural frequency, modal damping, mode shape

1. INTRODUCTION

Piezoceramic transducers have been widely applied and integrated into structures for active structural vibration and acoustic control.[1-7] Many researches have been dedicated to the development of the PZT actuation models [8-14] as well as the PVDF sensing models [15-19] for beams and plates. Crawley and de Luis [8] developed the PZT actuators adhered or embedded into cantilever beam for structural actuation. Dimitriadis et al. [9] extended their work to two-dimensional plate problem and derived the actuation force model for PZT pure-bending excitation. Im and Atluri [10] further considered the shear force and axial force effects for PZT actuator applied to beam structures. Wang and Rogers [11,12] applied the classical laminate plate theory to model the embedded PZT actuator for beams and plates, respectively, considering pure-bending, pure-extension and asymmetric excitation modes. Gibbs and Fuller [13] also derived the asymmetric PZT actuator excitation for beam structural vibration control.

The rectangular shape of PVDF film was introduced by Hubbard [15] for the application to vibration control of beam structures as the sensor. Lee and Moon [16] and Collin et al. [17] developed special shape of PVDF film to sense the specific vibration modal response as known modal sensors. Collet and Jezequel [18] and Tanaka et al. [19] utilized the similar configuration of PVDF film as modal filters for vibration control. The applications of PZT actuator and PVDF sensor integrated with structures, so called smart structure system, to structural vibration and acoustic control is very promising.

The idea of smart structural testing is also of interest and leads to structural fault diagnosis and health monitoring.[20] Sun et al. [21] derived the frequency response function (FRF) through electric admittance of piezoceramic transducers for obtaining the dynamic parameters of beam structures. However, they did not physically interpret those dynamic parameters. Norwood [22] successfully applied both the impact hammer and PVDF film, respectively, as actuation sources for the modal testing of cylindrical shell structures. Wang [23] derived the frequency response functions between the traditional and piezoceramic transducers for simply supported beam. He introduced the feasibility of the use of piezoceramic transducers for structural modal testing. Wang and Wang [24] theoretically and experimentally demonstrated the rectangular shape of PZT actuator and PVDF sensor for cantilever beam modal testing. They showed that the system modal parameters, including

*Correspondence: Bor-Tsuen Wang: wangbt@mail.npust.edu.tw; Telephone: 886-8-770-3202 ext. 7017; Fax: 886-8-774-0142

natural frequencies, modal damping ratios and structural mode shapes, can be properly extracted. Wang [25] further developed the modal analysis for the use of various forms of actuators and sensors. The FRFs can be derived and expressed in conventional modal format. The actuator and sensor mode shape functions are defined and interpreted according to types of actuators and sensors as well as the testing procedure.

This work intends to use the PZT actuator and PVDF sensor instead of traditional transducers, such as the impact hammer or shaker and accelerometer, for modal testing of simply supported plate. Huang et al. [26] developed an identification algorithm base on modal equations for a thin plate using the piezoceramic transducers. They did extract the natural frequencies and modal damping ratios of the plate but lack of structural mode shapes. This paper first develops the FRFs between the PZT actuator and PVDF sensor applied to the simply supported plate. The simply supported plate is constructed as Ochs and Snowdion [27] suggested and has been shown for the correctness of the test structure by conventional modal testing. [28] A series of rectangular shape of PVDF films are evenly distributed over the plate and act as the sensing devices instead of traditional acceleration sensors. The rectangular PZT patches that are adhered to the opposite surfaces of the plate and activated 180° out-of-phase for pure bending excitation are used as the actuator. The fixed PZT actuator location and roving the PVDF sensor location is adopted for experimental modal testing. A set of FRFs is measured and processed through modal parameter extraction method to determine the system modal parameters. Results show that modal frequencies, modal damping ratio and PVDF sensor mode shapes can be properly identified. In particular, for the simply supported boundary conditions the PVDF sensor mode shape is proportional to the displacement mode shape as demonstrated. The idea of smart structural testing is enhanced. The configuration of the system can also be applied to structural failure diagnosis.

2. THEORETICAL ANALYSIS

The thin plate theory is adopted, and the equation of motion for rectangular plate can be expressed as follows [29]:

$$D\nabla^2\nabla^2 w + \rho t_p \frac{\partial^2 w}{\partial t^2} + \bar{c}\frac{\partial w}{\partial t} = f(x,y,t) \tag{1}$$

where

$$D = \frac{E_p t_p{}^3}{12(1-\nu^2)} \tag{2}$$

$$\nabla^2 = \frac{\partial^2}{\partial x^2} + \frac{\partial^2}{\partial y^2} \tag{3}$$

$f(x,y,t)$ is the external force; w is the transverse displacement of plate; ρ plate density; t_p plate thickness; $\bar{c}$ damping coefficient per unit area; E_p Young's modulus of plate; ν Poison ratio of plate. To perform theoretical modal analysis, one can obtain the plate natural frequencies and their corresponding mode shapes as follows [29]:

$$\phi_{mn}(x,y) = \phi_m(x)\phi_n(y) = \sin\alpha_m x \sin\alpha_n y \tag{4}$$

$$f_{mn} = \frac{\omega_{mn}}{2\pi} = \frac{\pi}{2}\left[\frac{m^2}{L_x^2} + \frac{n^2}{L_y^2}\right]\sqrt{\frac{D}{\rho t_p}} \tag{5}$$

2.1. Harmonic analysis of PZT actuator excitation

Consider the actuation of the rectangular shape of PZT actuator as shown in Figure 1. Two PZT patches are adhered to the opposite sides of the plate symmetrically and activated 180º out-of-phase by a voltage input. The pure bending excitation can be activated. The equivalent force can be derived as distributed line moments along the four edges and expressed as follows [9]:

$$\begin{aligned} f(x,y,t) = {} & M_{eq}\left[\delta'(x-x_{c_{1j}}) - \delta'(x-x_{c_{2j}})\right]\left[H(y-y_{c_{1j}}) - H(y-y_{c_{2j}})\right]e^{i\omega t} \\ & + M_{eq}\left[H(x-x_{c_{1j}}) - H(x-x_{c_{2j}})\right]\left[\delta'(y-y_{c_{1j}}) - \delta'(y-y_{c_{2j}})\right]e^{i\omega t} \end{aligned} \tag{6}$$

where

$$M_{eq} = C_0\Lambda \tag{7}$$

$$\Lambda = \frac{d_{31}}{t_c}V_c \tag{8}$$

$\delta(x)$ is Delta function; $H(x)$ is the step function. $x_{c_{1j}}$, $x_{c_{2j}}$, $y_{c_{1j}}$, $y_{c_{2j}}$ represent the location of the *j*-th PZT actuator in both *x*- and *y*-coordinates. M_{eq} is the equivalent line moment. C_0 is functions of geometric and material constants for both PZT patch and plate. Λ is the piezoelectirc strain produced by the applied voltage V_c. d_{31} is the piezoelectric dielectric strain constant. t_c is the thickness of PZT patch.

The system response can also be harmonic and derived as follows:

$$w(x,t)=\sum_{m=1}^{\infty}\sum_{n=1}^{\infty}W_{mn}\phi_m(x)\phi_n(y)e^{i\omega t} \tag{9}$$

where

$$W_{mn}=\frac{-(\frac{1}{\alpha_m^2}+\frac{1}{\alpha_n^2})M_{eq}\left[\phi_m'(x_{c_{2j}})-\phi_m(x_{c_{1j}})\right]\left[\phi_n'(y_{c_{2j}})-\phi_n(y_{c_{1j}})\right]}{(\frac{L_x}{2}\frac{L_y}{2})\left[D(\alpha_m^2+\alpha_n^2)^2-\omega^2\rho t_p+i\omega\bar{c}\right]} \tag{10}$$

$$\phi_m'(x_{c_{2j}})-\phi_m'(x_{c_{1j}})=-2\alpha_m\sin\alpha_m\frac{l_{cx}}{2}\phi_m(x_{c_j}) \tag{11}$$

$$\phi_n'(y_{c_{2j}})-\phi_n'(y_{c_{1j}})=-2\alpha_n\sin\alpha_n\frac{l_{cy}}{2}\phi_n(y_{c_j}) \tag{12}$$

(x_{c_j}, y_{c_j}) represents the central location of the PZT actuator. l_{cx} and l_{cy} represent the length and width of the PZT actuator. Equations (11) and (12) are the slope difference mode shape between two opposite edges of the PZT actuator and proportional to the displacement mode shape. The modal amplitude can also be expressed as follows:

$$W_{mn}=\frac{-4\alpha_m\alpha_n\sin(\alpha_m\frac{l_x}{2})\sin(\alpha_n\frac{l_y}{2})(\frac{1}{\alpha_m^2}+\frac{1}{\alpha_n^2})M_{eq}\phi_{mn}(x_{c_j},y_{c_j})}{\rho t_p(\frac{L_x}{2}\frac{L_y}{2})\left[(\omega_{mn}^2-\omega^2)+i2\xi_{mn}\omega_{mn}\omega\right]} \tag{13}$$

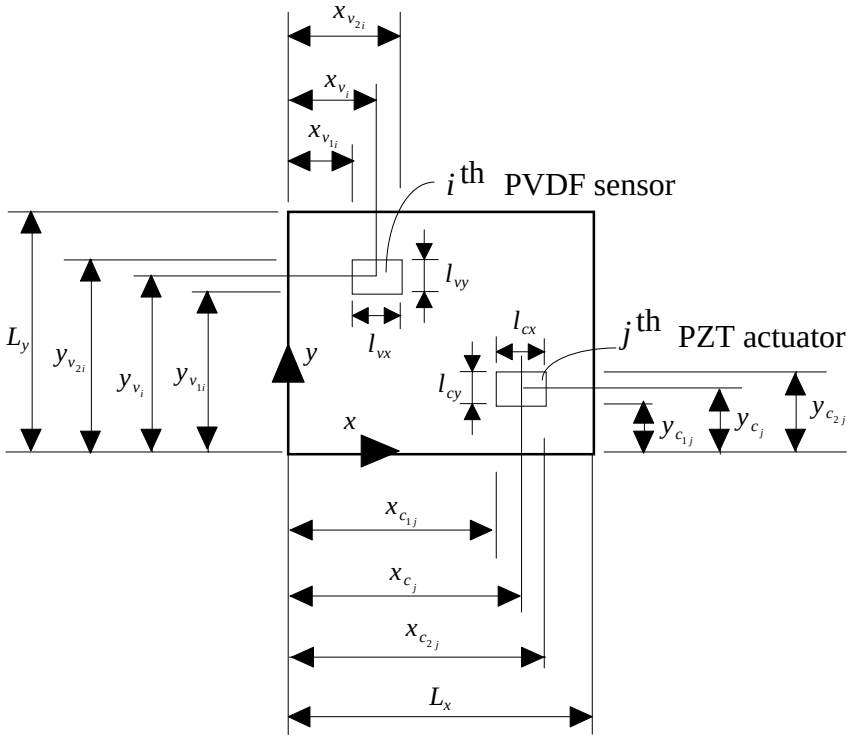

Figure 1. The arrangement of the *j*-th PZT actuator and the *i*-th PVDF sensor on the rectangular plate

where

$$\phi_{mn}(x_{c_j}, y_{c_j}) = \phi_m(x_{c_j})\phi_n(y_{c_j}) \tag{14}$$

2.2. Harmonic response of PVDF sensor

The shape function of the *i*-th PVDF sensor as shown in Figure 1 can be defined as follows:

$$\Gamma(x, y) = \left[H(x - x_{v1_i}) - H(x - x_{v2_i})\right]\left[H(y - y_{v1_i})H(y - y_{v2_i})\right] \tag{15}$$

where x_{v1_i}, x_{v2_i}, y_{v1_i}, y_{v2_i} are the location of the *i*-th PVDF sensor in *x*- and *y*-coordinates. The PVDF film sensing equation can be derived as follows [16]:

$$q(t) = (\frac{t_p + t_v}{2})\int_0^{L_x}\int_0^{L_y}\Gamma(x, y)(e_{31}\frac{\partial^2 w}{\partial x^2} + e_{32}\frac{\partial^2 w}{\partial y^2} + 2e_{36}\frac{\partial^2 w}{\partial x \partial y})dxdy \tag{16}$$

where t_v is the thickness of the PVDF film. e_{31}, e_{32}, e_{36} are piezoelectric field intensity constants. For the simply supported plate, torsional effect can be neglected, i.e., $e_{36} = 0$. The equation can be derived as follows:

$$q(t) = (\frac{t_p + t_v}{2})e^{i\omega t}\sum_{m=1}^{\infty}\sum_{n=1}^{\infty}W_{mn}(e_{31}\alpha_m^2 + e_{32}\alpha_n^2)\frac{1}{\alpha_m^2}\frac{1}{\alpha_n^2}\left\{\left[\phi_m^{'}(x_{v2_i}) - \phi_m^{'}(x_{v1_i})\right]\left[\phi_n^{'}(x_{v2_i}) - \phi_n^{'}(x_{v1_i})\right]\right\} \tag{17}$$

where

$$\phi_m'(x_{v_{2i}}) - \phi_m'(x_{v_{1i}}) = -2\alpha_m \sin\alpha_m \frac{l_{vx}}{2}\phi_m(x_{v_i}) \tag{18}$$

$$\phi_n'(y_{v_{2i}}) - \phi_n'(y_{v_{1i}}) = -2\alpha_n \sin\alpha_n \frac{l_{vy}}{2}\phi_n(y_{v_i}) \tag{19}$$

l_{vx} and l_{vy} are the length and width of the PVDF film, respectively, while x_{v_i}, y_{v_i} is the central location. Again, the PVDF sensor mode shape is the slope difference mode shape and proportional to the displacement mode shape for simply supported plate. The resultant voltage of the *i*-th PVDF sensor can be obtained:

$$V_{v_i}(t) = \frac{q(t)}{\varepsilon A_v}t_v \tag{20}$$

where ε is the permittivity of PVDF film. A_v is the PVDF sensor area. The resultant voltage can be rewritten:

$$V_{v_i}(t) = \frac{t_v}{\varepsilon A_v}(\frac{t_p + t_v}{2})e^{i\omega t}\sum_{m=1}^{\infty}\sum_{n=1}^{\infty}4\alpha_m\alpha_n W_{mn}\left[e_{31}\left(\frac{1}{\alpha_n}\right)^2 + e_{32}\left(\frac{1}{\alpha_m}\right)^2\right]\sin(\alpha_m\frac{L_{vx}}{2})\sin(\alpha_n\frac{L_{vy}}{2})\phi_{mn}(x_{vi}, y_{vi}) \tag{21}$$

2.3. Frequency response function

The frequency response function between the *i*-th PVDF sensor and the *j*-th PZT actuator can be derived and expressed in conventional modal format:

$$\alpha_{v_i f_j}(\omega) = \frac{V_{v_i}}{V_{c_j}} = \sum_{n=1}^{\infty}\sum_{m=1}^{\infty}\frac{\phi_{mn,i}^{v}\phi_{mn,j}^{c}}{(\omega_{mn}^2 - \omega^2) + i(2\xi_{mn}\omega_{mn}\omega)} \tag{22}$$

where

$$\phi_{mn,j}^{c} = \frac{-4k_c\alpha_m\alpha_n\left(\frac{1}{\alpha_m^2} + \frac{1}{\alpha_n^2}\right)}{\sqrt{\rho t_p\left(\frac{L_x}{2}\frac{L_y}{2}\right)}}\sin\alpha_m\frac{l_{cx}}{2}\sin\alpha_n\frac{l_{cy}}{2}\phi_{mn}(x_{c_j}, y_{c_j}) \tag{23}$$

$$\phi_{mn,i}^{v} = \frac{4k_v\alpha_m\alpha_n\left[e_{31}\left(\frac{1}{\alpha_n^2}\right) + e_{32}\left(\frac{1}{\alpha_m^2}\right)\right]}{\sqrt{\rho t_p\left(\frac{L_x}{2}\frac{L_y}{2}\right)}}\sin(\alpha_m\frac{l_{vx}}{2})\sin(\alpha_n\frac{l_{vy}}{2})\phi_{mn}(x_{v_i}, y_{v_i}) \tag{24}$$

$$k_c = \frac{c_0 d_{31}}{t_c} \tag{25}$$

$$k_v = \frac{t_v}{\varepsilon A_v}\left(\frac{t_p + t_v}{2}\right) \tag{26}$$

$\phi^c_{mn,j}$ is the value of the PZT actuator mode shape function at position *j*, and $\phi^v_{mn,i}$ is the value of the PVDF sensor mode shape function at position *i*. In particular, both the PZT actuator and PVDF sensor mode shape functions are the slope difference mode shapes in sense. For simply supported boundary conditions, the slope difference mode shape can be shown as proportional to the displacment mode shape.

3. EXPERIMENTAL ANALYSIS

The objective of experimental modal analysis is to obtain the first four modes, i.e., *m*=2 and *n*=2. The grid of the plate is shown in Figure 2 and numbered up to 25. The PZT actuator is located at position 21, while the PVDF sensors are evenly distributed at every position. The test plate is shown in Figure 3. The test equipment layout is depicted in Figure 4. White noise random signal from signal generator (BK 3016) is input to voltage transformer (SQV3/500) to amplify about 90 times of voltage to be input to PZT actuator. The resultant voltage measured from the PVDF sensor is amplified and input to channel B. The dual channel FFT analyzer (BK3550) captures both the input and output voltage of the PZT actuator and PVDF sensor, respectively, and calculates the frequency response function. Let the PZT actuator be fixed, roving the PVDF sensors a total number of 25 sets of FRFs can be measured and transported to CADA-PC, a general purpose curve fitting software to extract the system modal parameters. Natural frequencies, modal damping ratios and PVDF mode shape functions of the simply supported plate can be extracted. The physical properties of the plate, PZT actuator and PVDF sensor are shown in Tables 1-3.

Table 1. Physical properties of plate

material	Steel
Length (L_x)	0.38 (m)
Width (L_y)	0.3 (m)
Thickness (t_p)	0.002 (m)
Density (ρ)	7870 (kg/m^3)
Young's modulus (E)	207×10^9 (N/m^3)
Poison ratio (ν)	0.292

Table 2. Physical properties of PZT actuator

type	G-1195
Length (l_{cx})	38 (mm)
Width (l_{cy})	19 (mm)
Thickness(t_c)	1.905 (mm)
Young's modulus(E_c)	6.3×10^{10} (N/m^2)
Density (ρ_c)	7650 (kg/m^3)
Poison ratio (ν_c)	0.28
Piezoelectric strain constant ($d_{31} = d_{32}$)	166×10^{-12} (m/V)

Table 3. Physical properties of PVDF sensor

type	DT1-028K
Length (l_{vx})	38 (mm)
Width (l_{vy})	19 (mm)
Thickness (t_c)	28×10^{-6} (m)
Young's modulus (E_c)	6.3×10^{10} (N/m^2)
Density(ρ_c)	1800 (kg/m^3)
Poison ratio (ν_c)	0.33
Piezoelectric field intensity constant ($e_{31} = e_{32}$)	54×10^{-3} (m/V)
Permittivity (ε)	106×10^{-12} (F/m)

4. RESULTS AND DISCUSSIONS

4.1. Verification of frequency response functions

Figures 5(a)-(b) show the FRFs for i=2, j=21 and i=16, j=21 respectively. Because the PZT actuator is located at position 21, and both sides of the plate is adhered with the PZT patches, the 21th PVDF sensor is ignored. In this work, i=16 is used for i=21. In Figure 5, the solid line denotes the experimental FRF, the dash line denotes the synthesized FRF derived from the extracted modal parameters, and the chain line denotes the theoretical FRF. One can observe that the synthesized FRF agrees well with experimental FRF. The 60 Hz electrical noise in experiments is eliminated. This indicates the correctness of curve fitting process. The resonance frequencies and the shape of FRFs show very good agreement between the theoretical and experimental FRFs. The coherence functions corresponding to experimental FRFs in Figure 5 are shown in Figure 6. Most values are near 0.9 except where the anti-resonance frequencies and 60 Hz harmonics occur. The small value of coherence function at low frequency range can be due to the limitation of dynamic range of FRF analyzer. Generally speaking, the measurement of FRFs is satisfactory and suitable for further curve fitting process to extract modal parameters of the simply supported plate.

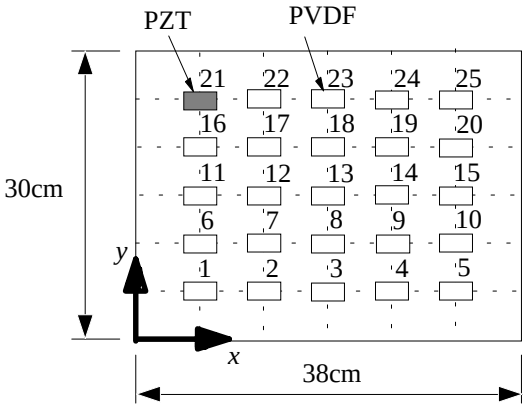

Figure 2. The division and number of simply supported plate

Figure 3. The test plate

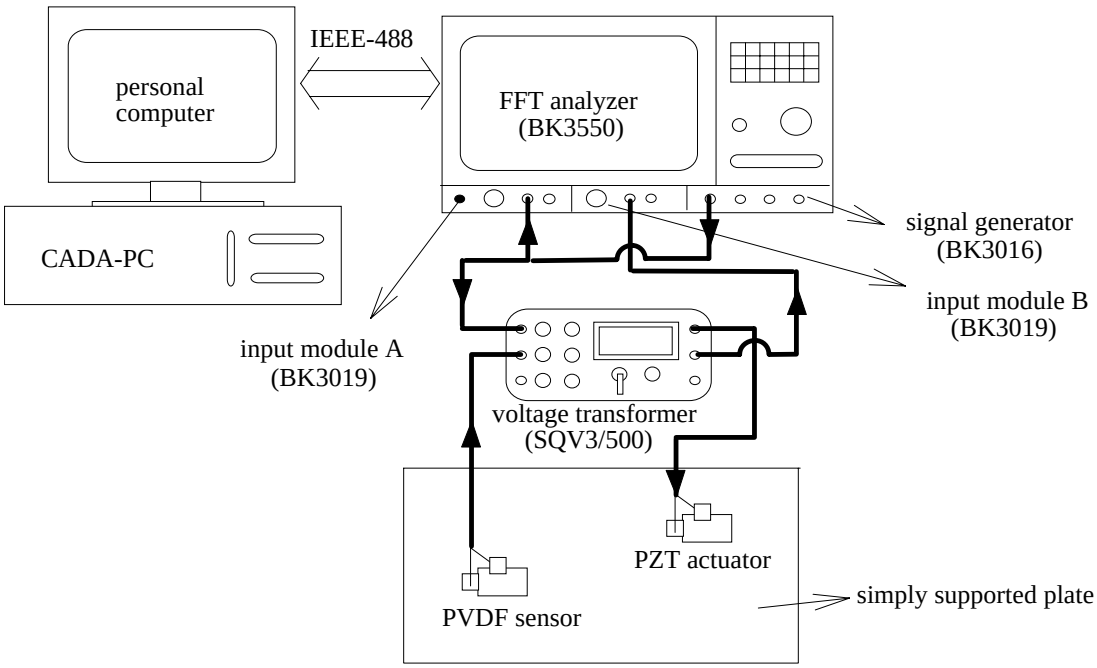

Figure 4. Experimental equipment layout

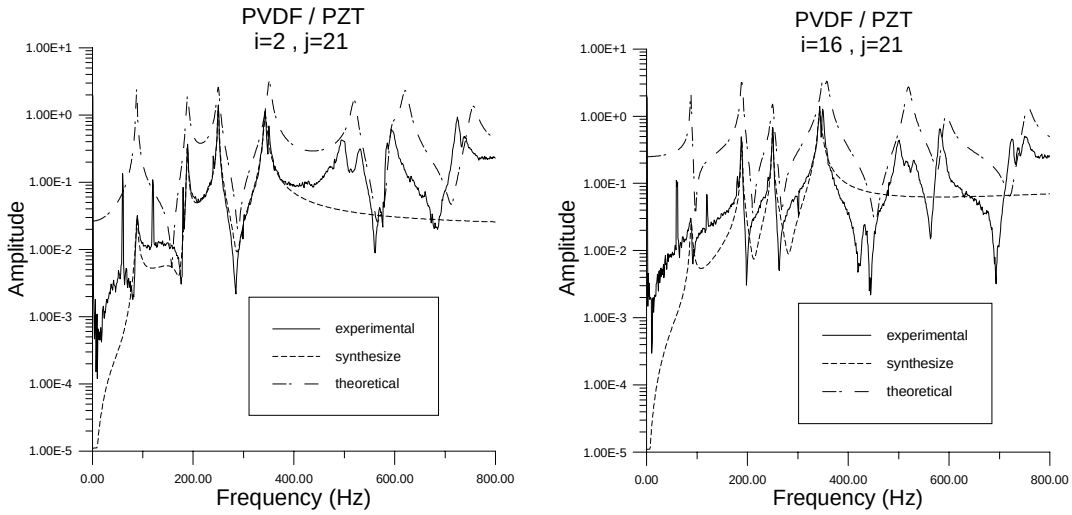

(a) i=2, j=21 (b) i=16, j=21

Figure 5. Frequency response functions

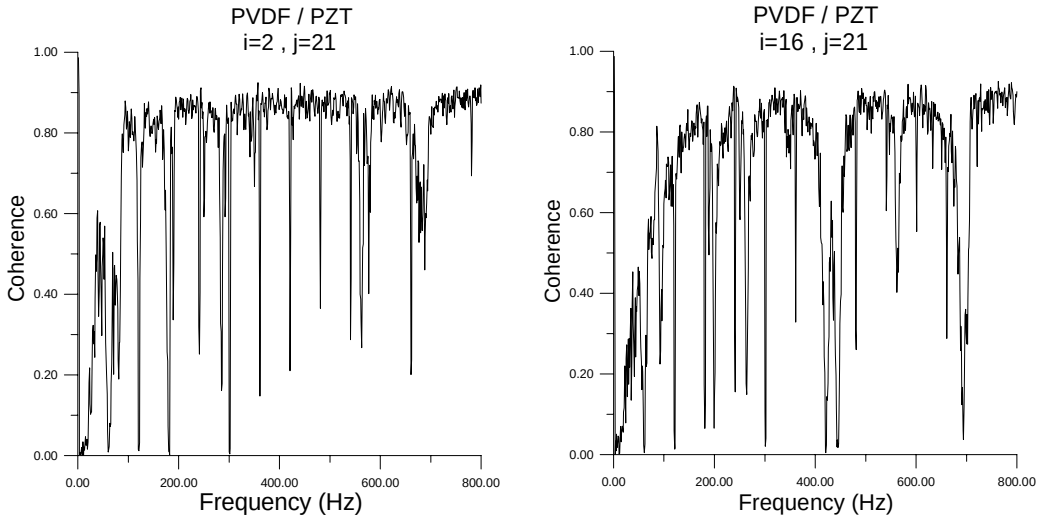

(a) i=2, j=21 (b) i=16, j=21

Figure 6. Coherence functions

4.2. Verification of modal parameters

Theoretical natural frequencies of the simply supported plate for m=5, n=5 are shown in Table 4. Table 5 shows the comparison of natural frequencies for the first four modes. The error percentage is less than –2.1%. The test plate is well simulated for the simply supported boundary conditions [28]. The piezoceramic transducers work well in predicting the natural frequencies of the structure.

Table 4. Natural frequencies of the simply supported plate (Hz)

m\n	1	2	3	4	5
1	87.71	249.81	519.98	898.22	1384.53
2	188.74	350.85	621.02	999.25	1485.56
3	357.13	519.23	789.40	1167.64	1653.95
4	592.88	754.98	1025.15	1403.39	1889.69
5	895.98	1058.08	1328.25	1706.48	2192.79

Table 5. Comparison of natural frequencies between theoretical and experimental results and modal damping

Natural frequency	Experimental (Hz)	Theoretical (Hz)	Error percentage (%)	Damping ratio	Damping ratio (%)
$f_{1,1}$	88.43	87.711608	0.819	$\xi_{1,1}$	1.95
$f_{2,1}$	188.44	188.744605	-0.1614	$\xi_{2,1}$	0.39
$f_{1,2}$	249.76	249.813438	-0.0214	$\xi_{1,2}$	0.35
$f_{2,2}$	343.22	350.846434	-2.1737	$\xi_{2,2}$	0.78

Damping value can not be obtained through theoretical modal analysis. The viscous damping ratio is assumed to be 0.01 for all modes to generate the theoretical FRFs. The modal damping ratios extracted from the curve fitting process for the first four modes are also listed in Table 5. $\xi_{1,1}$ is 1.95% higher than the expected damping ratio 0.1-0.5% for steel material [30]. Other modal damping ratios agree well. However, it should noted that the adhesion and material effect of the PZT patches and PVDF films can also contribute to increase damping but neglected in theoretical analysis.

The first four theoretical displacement mode shapes of the simply supported plate are depicted in Figure 7, and the experimental PVDF sensor mode shapes are shown in Figure 8. In Figure 8, the mode shapes are depicted in amplitude, so all values are positive. One can observe that there are certain degree of similarity between Figures 7 and 8. In particular, for Figure 9(d) mode (2,2) there are two peak values near 1/3 of plate length in *x*-coordinate at central line of *y*=15cm. This can be explained that the natural frequency of (3,1) mode is 357.13 Hz near mode (2,2) 350.85 Hz. A modal superposition effect is observed. The PVDF sensor mode shapes as shown previously are proportional to the displacement mode shapes and validated in Figure 8. The use of piezoceramic transducers for the experimental modal testing is demonstrated and shown promising.

MSF (modal scale factor) and MAC (modal assurance criterion) [31] between the theoretical and experimentally predicted mode shapes are tabulated in Tables 6 and 7 respectively. One can see that the diagonal terms except for mode (2,2) close to one indicates the agreement between the theoretical and predicted mode shapes. The off-diagonal terms near zero indicate the orthoganality of mode shapes. The bad agreement of mode (2,2) is due to the coupling mode effect of mode (3,1) as discussed above. In summary, the use of PZT actuator incorporated with the PVDF sensors does successfully perform experimental modal testing of simply supported plate. The modal parameters, including natural frequencies, modal damping ratios and PVDF sensor mode shapes, are obtained and physically interpreted. The modal information is useful for further applications in structural fault diagnosis as well as other applications such as structural vibration and acoustic control.

Table 6. MSF values between theoretical and experimentally predicted mode shapes

Mode	(1,1)	(2,1)	(1,2)	(2,2)
(1,1)	**0.9547+i0.0345**	-0.0125+i0.0691	0.0448-i0.0294	0.1075-i0.0556
(2,1)	0.0325-i0.0089	**-.9680+i0.0139**	-0.0597+i0.0055	-0.1111-i0.0593
(1,2)	0.1365+i0.014	0.0984+i0.0086	**0.9469+i0.1294**	-0.0374-i0.0291
(2,2)	-0.0537+i0.0585	-0.0514-i0.0015	0.1524-i0.0012	**-0.8257+0.3774**

Table 7. MAC values between theoretical and experimentally predicted mode shapes

Mode	(1,1)	(2,1)	(1,2)	(2,2)
(1,1)	**0.9114**	0.0002	0.002	0.0116
(2,1)	0.0011	**0.9365**	0.0036	0.0123
(1,2)	0.0186	0.0097	**0.8967**	0.0014
(2,2)	0.0029	0.0026	0.0232	**0.6818**

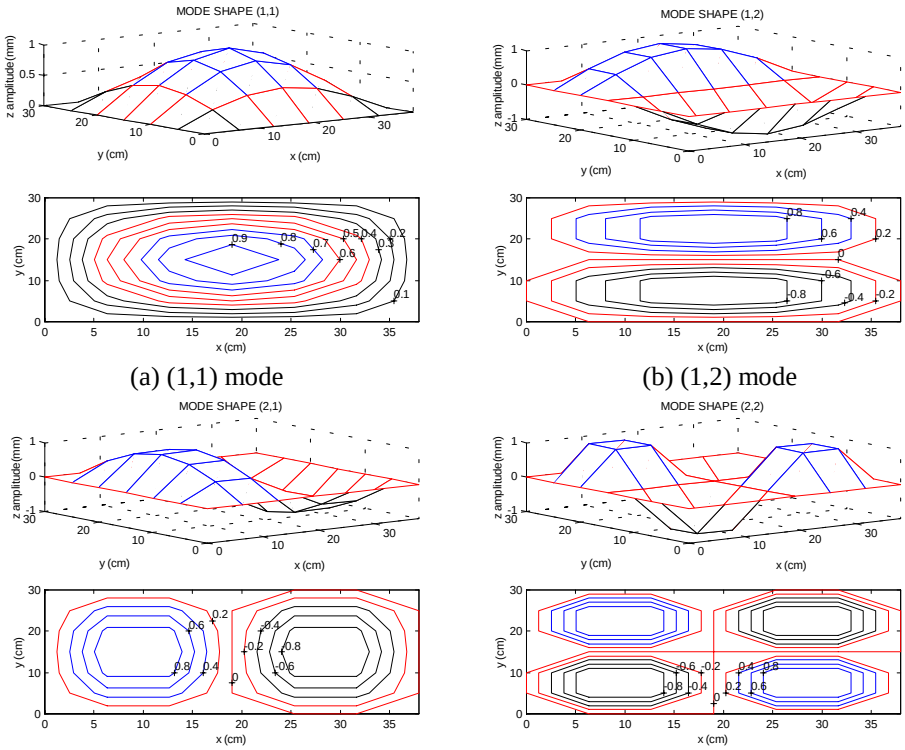

(a) (1,1) mode (b) (1,2) mode

(c) (2,1) mode (d) (2,2) mode

Figure 7. Theoretical displacement mode shape of the simply supported plate

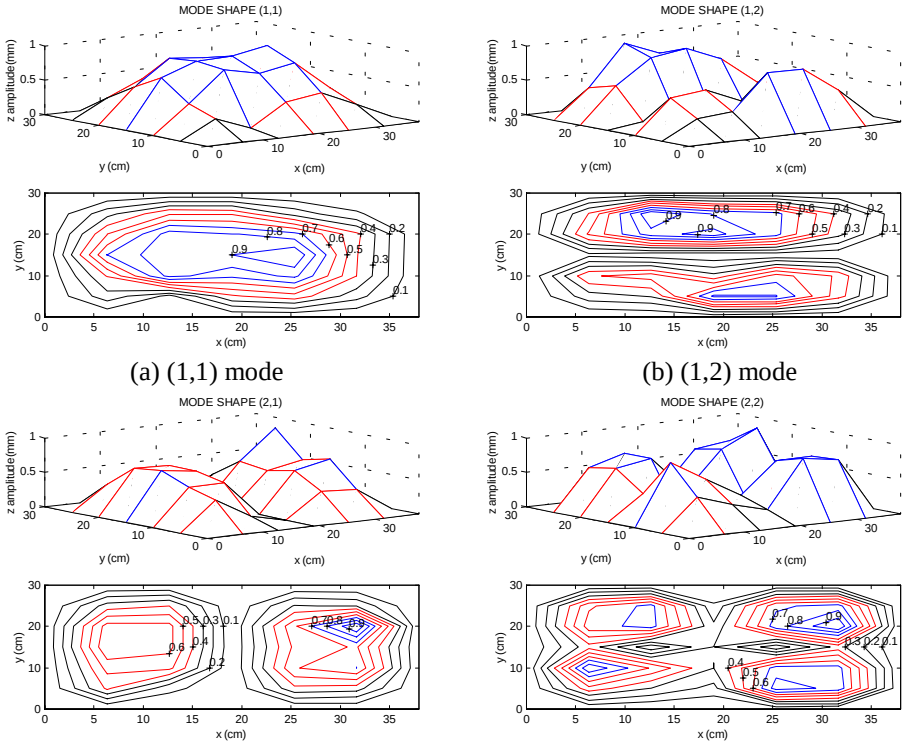

(a) (1,1) mode (b) (1,2) mode

(c) (2,1) mode (d) (2,2) mode

Figure 8. Experimental PVDF sensor mode shape of simply supported plate

5. CONCLUSIONS

This work adopts the PZT actuator and PVDF sensors to conduct the experimental modal testing for a simply supported plate. The theoretical modal analysis is first presented. The system frequency response function between the PZT actuator and PVDF sensor is also derived. The conventional experimental modal testing procedure is then performed with the use of piezoceramic transducers. The fixed PZT actuator and roving the PVDF sensor to measure FRFs is carried out. Since FRFs can be expressed in conventional modal format, the traditional modal parameter extraction methods can be applied. All of modal parameters, including natural frequencies, modal damping ratios and PVDF sensor mode shapes can be well identified and physically interpreted. In particular, the PVDF sensor mode shapes can be shown to be proportional to the displacement mode shapes. Through the comparison study of the FRFs and the extracted modal parameters, the idea of smart structural testing (SST) is demonstrated for its feasibility and validity. The smart structure system is also enhanced for its future applications in structural fault diagnosis as well as structural vibration and acoustic control.

ACKNOWLEDGEMENTS

The authors gratefully thank the financial support for this work from National Science Council of Republic of China under contract number: NSC89-2212-E-020-001.

REFERENCE

1. T. Bailey, and J. E. Hubbard, "Distributed Piezoelectric-Polymer Active Vibration Control of a Cantilever Beam," *AIAA Journal of Guidance Control*, **6**, pp. 605-611, 1985.
2. J. M. Plump, J. E. Hubbard, and T. Bailey, "Nonlinear Control of a Distributed System: Simulation and Experimental Results," *Journal of Dynamic System, Measurement, and Control*, **109,** pp. 133-139, 1987.
3. R. L. Clark, and C. R. Fuller, "A Model Reference Approach for Implementing Active Structural Acoustic Control," *Journal of Acoustical Society of America*, **6**, pp. 1534-1544, 1992.
4. R. L. Clark, R. A. Burdisso, and C. R. Fuller, "Design Approaches for Shaping Polyvinylidene Fluoride Sensors in Active Structural Acoustic Control," *Journal of Intelligent Material System and Structures*, **4**, pp. 354-365, 1993.
5. J. D'Cruz, "The Active Control of Panel Vibrations with Piezoelectric Actuators," *Journal of Intelligent Material Systems and Structures*, **4**, pp. 398-402, 1993.
6. A. J. Young, and C. H. Hansen, "Control of Flexural Vibration in a Beam Using a Piezoceramic Actuator and an Angle Stiffener," *Journal of Intelligent Material System and Structures*, **5**, pp. 536-549, 1994.
7. B. T. Wang, "Active Control of Far-Field Sound Radiation by a Beam: Physical System Analysis," *Smart Materials Structures*, **3**, pp. 476-484, 1994.
8. E. F. Crawley, and J. de Luis, "Use of Piezoelectric Actuators as Elements of Intelligent Structures," *AIAA Journal*, **25(10)**, pp. 1373-1385, 1987.
9. E. F. Dimitriadis, C. R. Fuller, and C. A. Rogers, "Piezoelectric Actuators for Distributed Vibration Excitation of Thin Plates," *Transactions of the ASME*, **113**, pp. 100-107, 1991.
10. S. Im, and S. N. Atluri, "Effects of a Piezo-Actuator on a Finitely Deformed Beam Subjected to General Loading," *AIAA Journal*, **27(12)**, pp. 1801-1807, 1989.
11. B. T. Wang, and C. A. Rogers, "Laminate Plate Theory for Spatially Distributed Induced Strain Actuators," *Journal of Composite Materials*, **25**, pp. 433-452, 1991.
12. B. T. Wang, and C. A. Rogers, "Modeling of Finite-Length Spatially Distributed Induced Strain Actuators for Laminate Beams Structures," *Journal of Intelligent Material Systems and Structures*, **2**, pp. 38-58, 1991.
13. G. P. Gibbs, and C. R. Fuller, "Excitation of Thin Beams Using Asymmetric Piezoelectric Actuators," *Journal of Acoustical Society of America*, **92(6)**, pp. 3221-3227, 1992.
14. R. L. Clark, C. R. Fuller, and A. Wicks, "Characterization of Multiple Piezoelectric Actuators for Structural Excitation," *Journal of Acoustical Society of America*, **90**, pp. 346-357, 1991.
15. J. E. Hubbard, 1987, "Distributed Sensors and Actuators for Vibration Control in Elastic Components," *Noise-Con 87*, pp. 407-412, 1987.
16. C. K. Lee, and F. C. Moon, "Modal Sensors/Actuators," *Journal of Applied Mechanics*, **57**, pp. 434-441, 1990.
17. S. A. Collins, C. E. Padilla, R. J. Notestine, A. H. von Flotow, E. Schmitz, and M. Ramey, "Design, Manufacture, and Application to Space Robotics of Distributed Piezoelectric Film Sensors," *Journal of Guidance Control*, **15**, pp. 396-403, 1992.
18. M. Collet, and L. Jezequel, "A New Approach to Modal Filtering with Laminated Piezo-electric Sensors," *Proceedings fo the 12th International Modal Analysis Conference*, pp.246-254, 1994.

19. N. Tanaka, S. D. Snyder, and C. H. Hansen,, "Distributed Parameter Modal Filtering Using Smart Sensors," *Transactions of the ASME Journal of Vibration and Acoustics*, **118**, pp. 630-640, 1996.
20. S. C. Galea, W. K. Chiu, and J. J. Paul, 1993, "Use of Piezoelectric Films in Detecting and Monitoring Damage in Composites," *Journal of Intelligent Material Systems and Structures*, **4**, pp. 330-336, 1993.
21. F. P. Sun, C. Liang, and C. A. Rogers, "Experimental Modal Testing Using Piezoceramic Patches as Collocated Sensor-Actuators," *Proceedings of the 1994 SEM Spring Conference and Exhibits*, pp. 871-879, 1994.
22. C. Norwood, "The Measurement of Natural Frequencies and Mode Shapes of Submerged Cylinders Using PVDF Strip Excitation," *Proceedings of Inter-Noise 95*, pp. 1337-1340, 1995.
23. B. T. Wang, "Characterization of Transfer Functions for Piezoceramic and Conventional Transducers," *Journal of Intelligent Material Systems and Structures*, **7,** pp. 390-398, 1996.
24. B. T. Wang, and C. C. Wang, "Feasibility Analysis of Using Piezoceramic Transducers for Cantilever Beam Modal Testing," *Smart Materials Structures*, **6**, pp. 106-116, 1997.
25. B. T. Wang, "Structural Modal Testing with Various Actuators and Sensors," *Mechanical Systems and Signal Processing*, **12(5),** pp. 627-639, 1998.
26. J. K. Huang, C. H. Choi, C. K. Song, and J. M. Lee, "Identification of a Thin Plate with Piezoelectric Actuators and Sensors," *Journal of Vibration and Acoustics*, **120,** pp.826-828, 1998.
27. J. B. Ochs, and J. C. Snowdion, "Transmissibility Accross Simply Supported Thin Plates. I. Rectangular and Square Plates with and without Damping Layers," *Journal of Acoustical Society of America*, **58(4),** pp. 832-840, 1975.
28. B. T. Wang, and R. L. Chen, "Experimental Modal Analysis of a Simply Supported Plate," *Bulletin of National Pingtung University of Science and Technology*, **6(4),** pp. 273-281, 1997. (in Chinese)
29. R. Szilard, *Theory and Analysis of Plates Classical and Numerical Methods*, Prentice-Hall, Inc., Englewood Cliffs, New Jersey, 1974.
30. C. M. Harris, and C. E. Crede, *Shock and Vibration Handbook*, McGraw-Hill Inc., 1976.
31. D. J. Ewins, *Modal Testing: Theory and Practice*, Research Studies Press LTD., Letchworth Hertfordshire, England, 1986.